Anti-SARS-CoV-2 activity of cyanopeptolins produced by *Nostoc edaphicum* CCNP1411

Robert Konkel [a,1], Aleksandra Milewska [b,1], Nguyen Dan Thuc Do [c], Emilia Barreto Duran [b], Artur Szczepanski [b], Jacek Plewka [b,d], Ewa Wieczerzak [e], Sofia Iliakopoulou [f], Triantafyllos Kaloudis [g,h], Dirk Jochmans [c], Johan Neyts [c], Krzysztof Pyrc [b,**,2], Hanna Mazur-Marzec [a,*]

[a] *Department of Marine Biology and Biotechnology, Faculty of Oceanography and Geography, University of Gdańsk, Gdynia, Poland*
[b] *Virogenetics Laboratory of Virology, Małopolska Centre of Biotechnology, Jagiellonian University, Kraków, Poland*
[c] *KU Leuven, Department of Microbiology, Immunology and Transplantation, Rega Institute, Laboratory of Virology and Chemotherapy, Leuven, Belgium*
[d] *Faculty of Chemistry, Jagiellonian University, Kraków, Poland*
[e] *Department of Biomedical Chemistry, Faculty of Chemistry, University of Gdańsk, Gdańsk, Poland*
[f] *Department of Sustainable Agriculture, University of Patras, Agrinio, Greece*
[g] *Institute of Nanoscience & Nanotechnology, NCSR Demokritos, Agia Paraskevi, Greece*
[h] *Laboratory of Organic Micropollutants, Water Quality Control Department, EYDAP SA, Menidi, Athens, Greece*

ARTICLE INFO

ABSTRACT

Despite the advances in contemporary medicine and availability of numerous innovative therapies, effective treatment and prevention of SARS-CoV-2 infections pose a challenge. In the search for new anti-SARS-CoV-2 drug candidates, natural products are frequently explored. Here, fifteen cyanopeptolins (CPs) were isolated from the Baltic cyanobacterium *Nostoc edaphicum* and tested against SARS-CoV-2. Of these depsipeptides, the Arg-containing structural variants showed the strongest inhibition of the Delta SARS-CoV-2 infection in A549$^{ACE2/TMPRSS2}$ cells. The functional assays indicated a direct interaction of the Arg-containing CP978 with the virions. CP978 also induced a significant decline in virus replication in the primary human airway epithelial cells (HAE). Of the four tested SARS-CoV-2 variants, Wuhan, Alpha, Omicron and Delta, only Wuhan was not affected by CP978. Finally, the analyses with application of confocal microscopy and with the SARS-CoV-2 pseudoviruses showed that CP978-mediated inhibition of viral infection results from the direct binding of the cyanopeptolin with the coronaviral S protein. Considering the potency of viral inhibition and the mode of action of CP978, the significance of the peptide as antiviral drug candidate should be further explored.

1. Introduction

As the severe acute respiratory syndrome coronavirus 2 (SARS-CoV-2) pandemic unfolded at the onset of the 2020s, the urgent demand for novel antiviral drugs became abundantly clear to both medical professionals and the general public. During two years, the virus spread to all parts of the globe and caused 6,938,353 confirmed deaths (WHO, entry 31.05.23), but the estimated true death toll reached 20, 000, 000 (COVID-19 Excess Mortality Collaborators, 2022). A year after the emergence of SARS-CoV-2, a large-scale vaccination operation was initiated as a strategy to curb the impact of the pandemic. Concurrently, the evolution of SARS-CoV-2 yielded multiple variants differing in transmissibility, severity, and public health impact. The effectiveness of the vaccines developed against the variants varied and the protection waned over time, especially in older and immunocompromised individuals (Cao et al., 2022; Zeng et al., 2022). Therefore, simultaneously with vaccination campaigns, efforts to develop new therapies were intensified. Regrettably, the success rate has been low, and so far only a

---

* Corresponding author.
** Corresponding author.
E-mail addresses: k.a.pyrc@uj.edu.pl (K. Pyrc), hanna.mazur-marzec@ug.edu.pl (H. Mazur-Marzec).
[1] RK and AM contributed equally to all aspects of the article.
[2] www.http://virogenetics.info/

few drugs showed limited efficacy (Beigel et al., 2020; Yip et al., 2022), with a notable exception of paxlovid, which showed almost 1 log reduction in mortality among high-risk patients (Liu et al., 2023). Promising drug candidates predominantly target viral components, such as the spike (S) glycoprotein, the cysteine proteases (M[pro]/3CL[pro] and PL[pro]), RNA-dependent RNA polymerase (RdRp) and the angiotensin converting enzyme 2 (ACE2) of the host cell (Krumm et al., 2021). Other potential treatments aim to alleviate infection symptoms and facilitate recovery by modulating the improper and excessive immune responses (Rommasi et al., 2022). Among the screened compounds that target these elements, numerous natural products such as isoprenoids, alkaloids, amides, tannins, peptides, and polyketides have been identified (da Silva Antonio et al., 2020; Wang et al., 2022; Chhetri et al., 2022; Raman et al., 2022; Al-Harrasi et al., 2022; Vargas et al., 2023). They come from organisms representing different phyla and habitats. These products of plants, animals, fungi and bacteria, with their enormous structural diversity and unique biological activities, represent well-documented potential to aid in the prevention and treatment of viral infections. In the case of cyanobacteria, the activity of lectins and polysaccharides against enveloped viruses has been studied for more than two decades (Mazur-Marzec et al., 2021; Mitchell et al., 2017; Mader et al., 2016). In a significant part of the works, the antiviral potential of cyanometabolites synthesised by strains of the *Nostoc* genus was demonstrated (Carpine and Sieber, 2021). Cyanovirin-N (CV–N), a lectin isolated from *N. ellipsosporum,* acts by blocking the interaction between the human immunodeficiency virus (HIV) gp120 and the CD4 T-cell receptor (Barrientos & Gronenborn, 2005; Liu et al., 2009). CV-N is also active against other enveloped viruses with glycoprotein containing *N*-linked high mannose oligosaccharides (Barrientos et al., 2003). Nostoflan, the acidic polysaccharide produced by *N. flagelliforme* inhibited the replication of herpes simplex virus (HSV), human cytomegalovirus (HCMV) and influenza viruses, preventing the binding of the virus to host cells. This polysaccharide also augments the host's immune defence mechanisms (Kanekiyo et al., 2007). In a limited number of studies, the potential of cyanometabolites to inhibit coronavirus infection was explored. Naidoo et al. (2020), analysed the conformational stability of the complexes formed by the interaction of 23 cyanometabolites with M[pro] and PL[pro]. Based on the binding energy scores of the complexes as well as other physicochemical properties, deoxycylindrospermopsin was recommended as the promising coronavirus protease inhibitor. In another computational study, conducted in parallel with ADME and toxicity tests, photoprotective mycosporine-glycine-valine and shinorine (scytonemin) effectively interacted with the ACE2 receptor (Sahu et al., 2022). *In silico* docking was also used to study the interaction between the receptor binding domain of the viral S protein and the *Arthrospira* products, phycoerythrobilin, phycocyanobilin, phycourobilin and folic acid, (Petit et al., 2021). Zainuddin et al. (2007) showed that chromatographic fractions containing ichthyopeptins A and B, the structural analogues of cyanopeptolins (CPs), were active against the influenza A virus. Cyanopeptolins are also produced by the Baltic cyanobacterium *Nostoc edaphicum* CCNP1411 (Mazur-Marzec et al., 2018), These compounds, categorised as cyclic depsipeptides with the 3-amino-6-hydroxy-2-piperidone (Ahp) moiety, were reported to inhibit serine proteases (trypsin, chymotrypsin, thrombin and plasmin (Gesner-Apter and Carmeli, 2009; Gademann et al., 2010; Mazur-Marzec et al., 2018). During SARS-CoV-2 infection, host (e.g. TMPRSS2, furin and cathepsin) and viral (e.g. PL[pro] and M[pro]) proteases play an important role in virus entry to host cell or in the synthesis of viral non-structural proteins, respectively. Therefore, protease inhibitors are widely explored as potential antiviral drug candidates (Lv et al., 2022; Shapira et al., 2022; Saad et al., 2020). In the current study, the anti-SARS-CoV-2 activity of cyanopeptolins from *N. edaphicum* CCNP1411 was explored with the aim to select the most promising CP structural variants, identify their mechanism of action and determine the activity range against the SARS-CoV-2 variants.

2. Material and methods

2.1. Cyanobacterial material

Nostoc edaphicum CCNP1411 (GenBank accession no. **PRJNA638531**), isolated from the coastal water of the Baltic Sea, was grown for biomass in Z8 medium (7 PSU) (Kotai, 1972) at 20 ± 2 °C and continuous irradiation of 10 ± 2 µmol photons/m^2/s. After approximately three weeks, when the stationary state was reached, the cyanobacteria were harvested by centrifugation. The collected biomass was freeze-dried and stored in a desiccator before further analyses.

2.2. Extraction and isolation

Dry cyanobacterial biomass (150 g) was homogenised by grinding and extracted five times with 75% methanol (MeOH) in MilliQ water (5 × 1 l) by vortexing (15 min) and sonication in ultrasonic bath (10 min). The collected extracts were centrifuged (10,000 × *g*, 15 min, 4 °C) and diluted with MilliQ water to MeOH concentration <10%. To separate the extract into fractions and isolate pure compounds, flash chromatography followed by preparative chromatography were performed with a Shimadzu HPLC instrument (Shimadzu Corporation, Kyoto, Japan) equipped with a photodiode array detector (PDA) and a fraction collector. First, the sample was loaded onto a preconditioned 120 g SNAP KP-C18-HS flash chromatography column (Biotage, Uppsala, Sweden). Compounds were eluted with a step gradient from 0% to 100% MeOH in water, at a flow rate of 12 ml/min, and 40 ml fractions were collected. The procedure was repeated separately for each portion of the extract obtained from approx. 15 g d.w. The fractions containing cyanopeptolins (eluted with 40–100% MeOH) were further individually separated in a Jupiter Proteo C12 column (21.2 × 250 mm; 4 µm; 90 Å; Phenomenex, Aschaffenburg, Germany). During subsequent preparative runs, a mixture of 5% acetonitrile (ACN) in water (phase A) and 100% ACN (phase B), both containing 0.1% formic acid were used as an eluent. To isolate pure CP978, the content of phase B increased from 15% to 19% in 10 min, then to 20% in 10 min and to 29% in 20 min. The flow rate was 12 ml/min. The modified gradients used for the isolation of other CPs are shown in Table S1.

2.3. LC-MS/MS analysese

The fractionation and purification process was controlled using a system composed of an Agilent 1200 Series LC (Agilent Technologies, Waldbronn, Germany) and a QTRAP5500 mass spectrometer (Applied Biosystems, Sciex, Concord, ON, Canada). Separation of cyanopeptolins was performed in a Jupiter Proteo C12 column (4.6 × 150 mm; 4 µm; 90 Å; Phenomenex, Aschaffenburg, Germany). The mobile phase components and the gradient were the same as in the case of preparative runs, but the flow rate was 0.6 ml/min. Mass spectrometer operated in positive mode, at Turbo Spray source temperature 550 °C and ionisation voltage 5.5 kV. Spectra were acquired in information-dependent acquisition (IDA) mode. An enhanced product ion (EPI) was triggered when the pseudomolecular ion *m/z* was within the range of 500–1250 and the ion intensity exceeded 5×10^5 cps. The collision energy (CE) was 60 eV and the declustering potential (DP) was 80 eV. Data acquisition and processing were performed using Analyst QS (version 1.7.1, 2019, Applied Biosystems/MDS Analytical Technologies, Concord, ON, Canada).

For the measurements of the exact masses of cyanopeptolins, a high resolution tandem mass spectrometer was utilised. Chromatographic separation of CCNP1411 extract was accomplished in an Elute HPG1300 HPLC system (Bruker Daltonics, Bremen, Germany) using an Atlantis T3 C18 column (2.1 mm × 100 mm; 3 µm; 100 Å; Waters, Milford, Massachusetts, U.S.) with a VanGuard cartridge holder (precolumn, Waters, Milford, Massachusetts, USA). The mobile phases were water (A) and ACN (B) both acidified with 0.1% formic acid. The gradient elution

program was: 75% A (held for 2 min), to 100% B in 18 min (held for 3 min) and 75% in 1 min (held for 5 min) for equilibrium. The flow rate was 0.2 ml/min, column temperature was 30 °C and the injection volume was 10 µl. An Impact II high resolution time of flight tandem mass spectrometer (Q-ToF-MS) (Bruker Daltonics, Bremen, Germany) equipped with an electrospray ionisation source operated in positive mode was used. The ESI capillary voltage was 3.1 kV and the collision energy ranged from 8.4 eV to 10.5 eV (25%–75% of the timing). Full scan accurate mass spectra were obtained in the m/z range 50–1300 in Auto MS (Data Dependent Analysis, DDA) with dynamic exclusion. Bruker's HyStar and Data Analysis software were used for data acquisition and to convert HRMS data to mzXML files, for further data analyses.

2.4. NMR analyses

The 1D ^{1}H NMR and 2D homo- and heteronuclear NMR (COSY, TOCSY, ROESY, HSQC, and HMBC) were acquired with the application of a Bruker Avance III spectrometers, 500 MHz and 700 MHz. Spectra were recorded in dimethyl sulfoxide-d$_6$ (DMSO-d$_6$). NMR data were processed and analysed by TopSpin (Bruker, Billerica, MA, USA) and POKY software (Lee et al., 2021).

2.5. Cell culture

Vero E6 cells (*Cercopithecus aethiops*; kidney epithelial; ATCC: CRL-1586; USA) were maintained in Dulbecco's modified Eagle's medium (DMEM; Thermo Fisher Scientific, Waltham, Massachusetts, USA) supplemented with 5% heat-inactivated fetal bovine serum (FBS; Thermo Fisher Scientific), streptomycin and penicillin (100 µg/ml and 100 mU/ml, respectively).

A549 cells (adenocarcinoma human alveolar basal epithelial; ATCC: CCL-185; USA) overexpressing ACE2 and TMPRSS2 (A549$^{ACE2/TMPRSS2}$ in-house generated (Synowiec et al., 2021) were maintained in DMEM medium (Gibco, Thermo Fisher Scientific) supplemented with 5% heat-inactivated fetal bovine serum (Gibco, Thermo Fisher Scientific) and penicillin-streptomycin solution (100 U/ml and 100 µg/ml, respectively; PAN Biotech GmbH, Aidenbach, Germany). Medium for the A549$^{ACE2/TMPRSS2}$ cells was additionally supplemented with blasticidin S (10 µg/ml; Sigma-Aldrich, Saint Louis, USA) and puromycin (0.5 µg/ml; Sigma-Aldrich).

2.6. Cytotoxicity assays

The XTT Cell Viability Assay kit (Biological Industries, Cromwell, USA) was used according to the manufacturer's instructions. Briefly, subconfluent A549$^{ACE2/TMPRSS2}$ cells were incubated in cyanopeptolin containing solution for 95 h at 37 °C, 5% CO$_2$. The medium was then discarded and fresh medium was overlaid on the cells, along with the activated 2,3-bis-(2-methoxy-4-nitro-5-sulphenyl)-(2H)-tetrazolium-5-carboxanilide (XTT) solution and cells were incubated for 2 h (37 °C, 5% CO$_2$). After this time, absorbance ($\lambda = 490$ nm) was measured using a microplate reader (SpectraMax iD5, Molecular Devices, San Jose, USA). The obtained results were further normalised to the control sample, where cell viability was set to 100%.

2.7. Human epithelium (HAE) cultures

Human airway epithelial cells (Epithelix SAS, Archamps, France) were maintained in BEGM medium. Before the test, cells were trypsinised and transferred to a permeable transwell insert supports ($f = 6.5$ mm). Cell differentiation was stimulated by medium additives. The removal of the media from the apical side was performed after the cells reached confluence. Cells were cultured for 3–5 weeks to form well-differentiated, pseudostratified mucociliary epithelia, as previously described (Milewska et al., 2020; Barreto-Duran et al., 2022).

2.8. Virus preparation and titration

SARS-CoV-2 isolates [original Wuhan (Munchen-1.2 2020/984), Alpha [B1.1.7], Omicron (B.1.1.529) and Delta isolate (B.1.617.2)] were generated by infecting monolayers of Vero E6 cells. The virus-containing liquid was collected on day 3 postinfection (p.i.), aliquoted, and stored at −80 °C. Control Vero E6 cell lysate from mock-infected cells was prepared in the same manner. Plates were incubated at 37 °C for 3 days, and the cytopathic effect (CPE) was scored by observation under an inverted microscope. Virus yield was assessed by titration on fully confluent Vero E6 cells in 96-well plates, according to the method of Reed and Muench (1938).

2.9. Virus infection

Unless stated otherwise, in all anti-SARS-CoV-2 assays the Delta variant was used.

2.9.1. Standard antiviral assays

In *in vitro* experiments, fully confluent A549$^{ACE2/TMPRSS2}$ cells in 96-well plates were exposed to either SARS-CoV-2 or a mock treatment at a 50% tissue culture infective dose (TCID$_{50}$) of 800 per ml in the presence of tested cyanopeptolin or control medium. After 2 h incubation at 37 °C, unbound virions were removed by washing with 100 µl of PBS and fresh medium containing dissolved respective cyanopeptolin variant was added to each well. Cell culture supernatants were collected on day 3 p.i. and analysed using reverse transcription-quantitative PCR (RT-qPCR). For the *ex vivo* study, fully differentiated human airway epithelium cultures were exposed to the tested cyanopeptolin or the control (PBS) for 30 min at 37 °C, following inoculation with SARS-CoV-2 at a TCID$_{50}$ of 800 per ml in the presence of the CP978 or control PBS. After 2 h incubation at 37 °C, unbound virions were removed by washing with 200 µl of PBS, and HAE cultures were maintained at the air-liquid interphase till the end of the experiment. To analyse the kinetics of the virus replication, each day p.i., 100 µl PBS was applied on the apical surface of the HAE and collected after a 10-min incubation at 37 °C. All samples were stored at −80 °C and analysed using RT-qPCR.

2.9.2. Functional tests

2.9.2.1. *Attachment assays.* Cells were incubated with 100 µl of CP978 (50 µg/ml) or DMSO in growth media for 60 min at 37 °C. Cells were then washed three times with PBS and infected with 100 µl SARS-CoV-2 (at TCID$_{50}$ = 800/ml). After four days of infection at 37 °C, supernatants were collected, and the number of SARS-CoV-2 RNA copies was determined using RT-qPCR.

2.9.2.2. *Entry assays.* Pre-cooled A549$^{ACE2/TMPRSS2}$ cells were inoculated with ice-cold SARS-CoV-2 at TCID$_{50}$ of 800/ml and incubated at 4 °C for 2 h to allow virus binding. Next, the virus particles were removed by washing with ice-cold 1 × PBS and cells were incubated with cyanopeptolin CP978 (50 µg/ml) or control DMSO at 37 °C for 2 h to allow virus penetration and to evaluate whether the cyanopeptolin interferes with this process. Subsequently, the media were removed and cells were washed 3 times with an acidic buffer in order to inhibit the fusogenic activity of the virions that were not internalised. The efficiency of virus deactivation using low pH was verified prior to these experiments. Subsequently, cells were washed with 1 × PBS, overlaid with culture medium and incubated at 37 °C for four days.

2.9.2.3. *Adsorption assays.* Cells were pre-cooled at 4 °C, overlaid with 100 µl of CP978 (50 µg/ml) and SARS-CoV-2 (TCID$_{50}$ = 800/ml). Cells were incubated at 4 °C to allow virus attachment, but not the internalisation to the host cell. Cells were then washed three times with PBS, and 100 µl of fresh medium was added. Cells were incubated for 4 day at

37 °C, and then, supernatants were collected for RT-qPCR analyses.

2.9.2.4. Release assays. Cells were infected with 100 μl SARS-CoV-2 at (TCID$_{50}$ = 800/ml) and incubated for 2 h at 37 °C to allow the virus to enter the cells. After incubation, cells were rinsed three times with PBS, and 100 μl of CP978 (50 μg/ml) or control (DMSO) in the growth medium was applied. Cells were incubated for 4 days at 37 °C, and supernatants were collected for RT-qPCR analyses.

2.9.2.5. Virus inactivation assays. SARS-CoV-2 virions were incubated with CP978 (50 μg/ml) or control (DMSO) for 60 min at room temperature. After preincubation, samples were titrated onto confluent A549$^{ACE2/TMPRSS2}$ cells. Plates were incubated at 37 °C for 4 days, and the cytopathic effects were scored by observation under an inverted microscope.

2.10. Isolation of nucleic acids and reverse transcription-quantitative PCR (RT-qPCR)

Isolation of viral RNA was carried out using a commercially available RNA isolation kit (Viral DNA/RNA Isolation Kit; A&A Biotechnology, Poland), according to the protocol provided by the manufacturer. The isolated RNA was subjected to RT-qPCR using the GoTaq® Probe 1-Step RT-qPCR System Protocol kit (Promega, Madison, Wisconsin, USA) according to the manufacturer's instructions with the use of primers and probes listed in Table 1. Appropriate standards were prepared to evaluate the number of viral RNA molecules in the samples. The reaction was carried out in a thermal cycler (CFX96 Touch Real-197 Time PCR Detection System; Bio-Rad, Hercules, California, USA). The obtained data are presented as log reduction value (LRV), showing the relative decrease in the amount of virus in cell culture media compared to the untreated sample.

2.11. Immunostaining and confocal imaging

Fixed cells were permeabilized with 0.1% Triton X-100 in PBS and incubated overnight at 4 °C in PBS supplemented with 5% bovine serum albumin (BSA) and 0.5% Tween 20. To visualise SARS-CoV-2 particles, cells were incubated for 2 h at room temperature with mouse anti-SARS-CoV-2 N IgGs (MA5-29981, Thermo Fisher Scientific, Waltham, Massachusetts, USA) (1 : 200 dilution), followed by 1 h incubation with Alexa Fluor 488-labelled goat anti-mouse IgG (Thermo Fisher Scientific, Waltham, Massachusetts, USA) (2.5 mg/ml). Nuclear DNA was stained with DAPI (49,6-diamidino-2-phenylindole) (Sigma-Aldrich, Saint Louis, USA) (0.1 mg/ml). Immunostained cultures were mounted on glass slides in ProLong Gold antifade medium (Thermo Fisher Scientific, Waltham, Massachusetts, USA). Fluorescent images were acquired under a Leica TCS SP5 II confocal microscope (Leica Microsystems GmbH, Mannheim, Germany) and a Zeiss LSM 710 confocal microscope (Carl Zeiss Microscopy GmbH, Jena, Germany). Images were acquired using Leica Application Suite Advanced Fluorescence LAS AF v. 2.2.1 software (Leica Microsystems CMS GmbH, Mannheim, Germany) or ZEN 2012 SP1 software (Carl Zeiss Microscopy GmbH, Jena, Germany) and were deconvolved with Huygens Essential package version 4.4 (Scientific Volume Imaging B.V., Hilversum, The Netherlands) and processed using ImageJ 1.47v (National Institutes of Health, Bethesda, USA).

Table 1
Oligonucleotides used for SARS-CoV-2 RT-qPCR.

Oligonucleotides	Sequence (5' -> 3')
5′ primer (Forward)	CACATTGGCACCCGCAATC
3′ primer (Reverse)	GAGGAACGAGAAGAGGCTTG
Fluorescent probe	6-ACTTCCTCAAGGAACAACATTGCCA-BHQ-1

2.12. Pseudovirus production and transduction

Human 293T cells (kidney epithelial cells ATCC: CRL-3216) were seeded in 10-cm diameter dishes, cultured for 24 h at 37 °C with 5% CO$_2$, and transfected using polyethylenimine (Sigma-Aldrich, Saint Louis, USA) with the lentiviral packaging plasmid (psPAX), the VSV-G envelope plasmid (pMD2G), or SARS-CoV-2 S glycoprotein (pCAGGS-SARS-CoV-2-S) and a third plasmid encoding firefly luciferase protein (pRRL luciferase). Cells were further incubated for 72 h at 37 °C with 5% CO$_2$, and pseudoviruses were collected every 24 h and stored at 4 °C. A549$^{ACE2/TMPRSS2}$ cells were seeded in 96-well plates, incubated for 24 h at 37 °C with 5% CO$_2$, and transduced with pseudoviruses harbouring VSV-G or S-SARS-CoV-2 proteins or lacking the fusion protein (ΔEnv) or in the presence of Polybrene (Sigma-Aldrich, Saint Louis, USA) (4 mg/ml) and CP978 or control (DMSO). After 4 h of incubation at 37 °C, the unbound virions were removed by three washes with PBS, and cells were further incubated for 72 h at 37 °C with 5% CO$_2$. After that, cells were lysed using Bright-Glo luciferase assay buffer (Promega, Poland) and transferred to white 96-well plates. Luminescence levels were measured on a SpectraMAx iD5 microplate reader (Molecular Devices, San Jose, California, USA).

2.13. Microscale thermophoresis (MST) assays

SARS-CoV-2 Spike (Omicron 6P spike ectodomain) was labelled with the Protein Labelling Kit RED-NHS 2nd Generation from NanoTemper Technologies, Inc. (San Francisco, California, USA) according to the manufacturer's guidelines. Labelled proteins were diluted in PBS containing 0.05% Tween-20 up to 10 nM and mixed with the tested nanobodies that were diluted twofold in the same buffer. The samples were allowed to incubate for 30 min at room temperature. Measurements were performed on a Monolith in duplicates using excitation power: 80% and MST power: medium in dedicated capillaries using RED nano detector. Data was further averaged and fitted with a kD fit using dedicated Nanotemper software (NanoTemper Technologies, San Francisco, California, USA). Hot and cold regions were set to 0 s and 0.5 s, respectively, to enhance the Temperature-Related Intensity Change (TRIC) as compared to the thermophoresis.

2.14. Statistical analysis

The Shapiro-Wilk test was used to evaluate normality of all data. When data showed normal distribution, one-way- or two-way-ANOVA was applied. When data did not show normal distribution the Kruskal-Wallis non-parametric test and Dunn's multiple comparison test were used.

3. Results

3.1. Isolation and CPs structure elucidation

Chromatographic runs yielded fifteen pure peptides. They were isolated in sufficient amounts to perform antiviral tests (Table 2). Structure elucidation of the peptides was based on the diagnostic ions present in the rich mass fragmentation spectra of [M+H]$^+$ (CPs with Arg^2) or [M + H – H$_2$O]$^+$ (CPs with Tyr^2, Phe^2 and Leu^2). These ions indicated the presence of specific residues and their sequences (Table S2). In the cyclic part, four residues were conserved: Thr^1, Ahp^3, Phe^4, Val^6, while in a side chain Asp^7 was always present. The most variable part of the structure was position 2 occupied by Arg^2 (eight CPs), Tyr^2 (three CPs), Phe^2 (two CPs) and Leu^2 (two CPs). Among the detected CPs, there were also two variants (CP922 and CP893), which lacked the fatty acid residue in the side chain. The diagnostic ions for CP978 are shown in Fig. 1. The purity of the isolated CP978 (>95%) was confirmed by LC-MS analysis (Figure S1).

Table 2

Cyanopeptolins isolated from *Nostoc edaphicum* CCNP1411 and tested in this study (Ahp – 3-amino-6-methoxy-2-piperidone, BA – butanoic acid, HA – hexanoic acid, Ac – acetyl group, MeTyr – *N*-methyltyrosine, diMeTyr – *N,O*-di-methyltyrosine, MePhe – *N*-methylphenylalanine, HRMS – *m/z* measured with a high resolution mass spectrometer, n.d. – not detected in cell extract).

Name	Exact CP mass	Calculated precursor ion (*m/z*)	HRMS (*m/z*)	Mass Error	Structure
CP 1020	1020.5280	1021.5359	1021.5350	0.0009	[Thr + Arg + Ahp + Phe + diMeTyr + Val]Asp + HA
CP 992	992.4967	993.5046	993.5043	0.0003	[Thr + Arg + Ahp + Phe + diMeTyr + Val]Asp + BA
CP 990	990.5175	991.5253	991.5246	0.0007	[Thr + Arg + Ahp + Phe + MePhe + Val]Asp + HA
CP 978	978.4811	979.4889	979.4889	0.0000	[Thr + Arg + Ahp + Phe + MeTyr + Val]Asp + BA
CP 964	964.4654	965.4733	965.4631	0.0001	[Thr + Arg + Ahp + Phe + diMeTyr + Val]Asp + Ac
CP 962	962.4862	963.4940	963.4939	0.0001	[Thr + Arg + Ahp + Phe + MePhe + Val]Asp + BA
CP 922	922.4549	923.4627	n.d.	–	[Thr + Arg + Ahp + Phe + diMeTyr + Val]Asp
CP 893	892.4443	893.4521	n.d.	–	[Thr + Arg + Ahp + Phe + MePhe + Val]Asp
CP 999	999.4590	982.4562	982.4555	0.0007	[Thr + Tyr + Ahp + Phe + diMeTyr + Val]Asp + BA
CP 985	985.4433	968.4406	968.4396	0.0010	[Thr + Tyr + Ahp + Phe + MeTyr + Val]Asp + BA
CP 969	969.4484	952.4457	952.4449	0.0008	[Thr + Tyr + Ahp + Phe + MePhe + Val]Asp + BA
CP 949	949.4797	932.4712	932.4764	0.0005	[Thr + Leu + Ahp + Phe + diMeTyr + Val]Asp + BA
CP 935	935.4640	918.4613	918.4610	0.0003	[Thr + Leu + Ahp + Phe + MeTyr + Val]Asp + BA
CP 983	983.4640	966.4613	966.4612	0.0001	[Thr + Phe + Ahp + Phe + diMeTyr + Val]Asp + BA
CP 953	953.4535	936.4507	936.4500	0.0007	[Thr + Phe + Ahp + Phe + MePhe + Val]Asp + BA
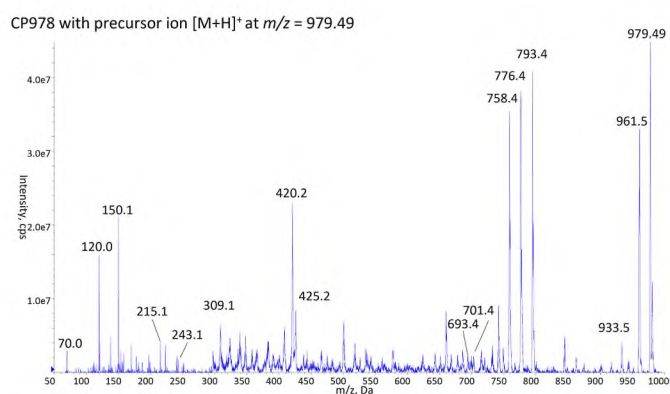
Fig. 1. The QTRAP5500 generated product ion mass spectrum of cyanopeptolin CP978 BA-Asp-[Thr-Arg-Ahp-Phe-MeTyr-Val] with the precursor ion [M+H]$^+$ at *m/z* 979.49. The mass signals were assigned to the following fragment ions: 961.5 [M + H − H$_2$O]$^+$, 933.5 [M + H − H$_2$O − CO]$^+$, 862.4 [M + H − Val − H$_2$O]$^+$, 793.4 [M + H − (BA + Asp)]$^+$, 776.4 [M + H − (BA + Asp) − H$_2$O]$^+$, 758.4 [M + H − (BA + Asp) − 2H$_2$O]$^+$, 701.4 [M + H − (Ahp + Phe) − H$_2$O]$^+$, 693.4 [Arg + Ahp + Phe + MeTyr + Val + H]$^+$, 425.2 [BA + Asp + Thr + Arg + H − H$_2$O]$^+$, 420.2 [Ahp + Phe + MeTyr + H − H$_2$O]$^+$, 309.1 [Phe(-N) + MeTyr + H]$^+$, 243.1 [Ahp + Phe + H − H$_2$O]$^+$, 215.1 [Ahp + Phe + H − H$_2$O − CO]$^+$, 150.1 MeTyr immonium ion, 120.0 Phe immonium ion, 70.0 Arg-related ion.

3.2. NMR analysis of CP978

To confirm the structure of the bioactive cyanopeptolin (CP978), NMR analyses were conducted. The ^{1}H NMR spectrum of the studied compound displayed a typical pattern of a peptide. The COSY, TOCSY and HMBC experiments allowed to assign the NMR spin systems to Asp, Thr, Arg, Ahp (3-amino-6-hydroxy-2-piperidone), Phe, MeTyr (*N*-methyl tyrosine), Val, and BA (butanoic acid) (Fig. 2). The amino acid sequence was confirmed by TOCSY data. The presence of two aromatic residues was recognised by the signals that occurred in the aromatic region of the spectrum (δ_H 6.77–7.17 ppm). One of them was identified as MeTyr based on the AA'BB' spin system between the aromatic protons (MeTyr-H2'/6' and MeTyr-H3'/5'). The ^{1}H–^{13}C long range correlation from the methyl group (δ_H 2.76 ppm) to the MeTyr-C2 atom (δ_C 61.3 ppm) revealed the presence of a *N*-methyl tyrosine residue. The second aromatic residue was found to be Phe based on the TOCSY interaction between proton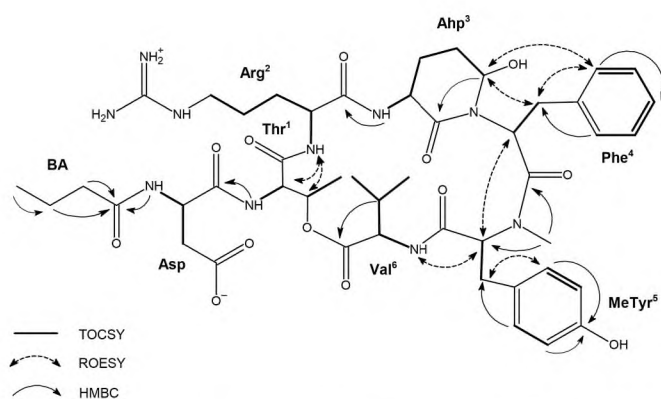s 2'/6', 3'/5', and 4', and the HMBC correlation from 3'/5' protons (δ_H 7.17 ppm) to the Phe-3 carbon atom (δ_C 35.8 ppm). The presence of Ahp residue was detected by the characteristic signal of the OH proton (δ_H 6.05 ppm) and a broad singlet (δ_H 5.06 ppm) derived

Fig. 2. Key TOCSY, ROESY, and HMBC correlations in cyanopeptolin CP978.

from the Ahp-H5 proton. The HMBC correlations from Ahp-H5 to Ahp-C1 confirmed the cyclic nature of this residue. The chemical shifts of the assigned proton and carbon atoms, and the complete set of ROESY and HMBC correlations are presented in Table S3, Figure S2-7.

3.3. Antiviral activity of CPs

The cytotoxic and anticoronaviral potential of different variants of cyanopeptolins produced by the Baltic strain CCNP1411 was analysed *in vitro*. The cytotoxicity of each compound at two concentrations: 100 and 50 μg/ml was tested on A549$^{ACE2/TMPRSS2}$ cells (Fig. 3). No significant cytotoxicity was observed for any of the tested cyanopeptides.

Next, the antiviral activity of CPs against SARS-CoV-2 (Delta variant) was analysed in a standard antiviral assay. The results are presented in Fig. 4.

Analyses showed a significant inhibition of the Delta SARS-CoV-2 infection in A549$^{ACE2/TMPRSS2}$ cells by several cyanopeptolins, especially those with Arg in position 2 (CP-Arg) (~2–3 logs). Cyanopeptolin CP978 was proven to be one of the most potent SARS-CoV-2 inhibitors. Due to antiviral potential and the fact that CP978 is synthesised by CCNP1411 in high quantities, this CP was chosen for further studies. Cytotoxicity and antiviral activity of CP978 was tested in a range of concentrations (0.1–100 μg/ml). In the virus infection assay, the determined inhibitory concentration (IC$_{50}$) was 80 ng/ml, with the significant SARS-CoV-2 inhibition already at the concentration of 1 μg/ml (Fig. 5).

Next, a series of functional assays was performed. The "Attachment assay" verified if CP978 interacts with the host cell and protects it from the infection, but no inhibition was observed. The "Entry assay" verified
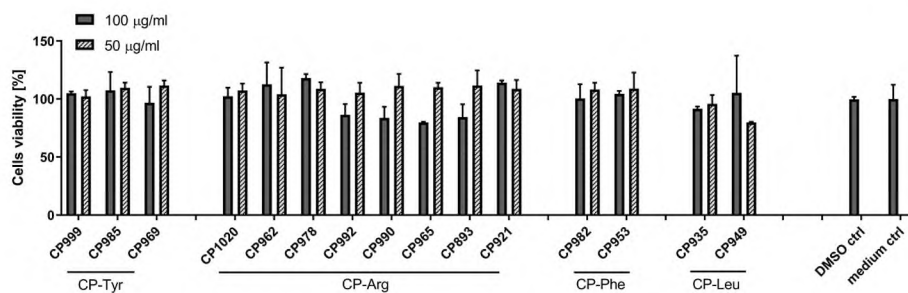
Fig. 3. The *in vitro* cytotoxicity of cyanopeptolins isolated from *Nostoc edaphicum* CCNP1411. Cell viability was assessed via XTT assay. Data on the y axis represent viability of the treated cells compared to the untreated reference samples. All assays were performed in triplicate and average values with standard errors are presented. The differences in cytotoxicity were not statistically significant.
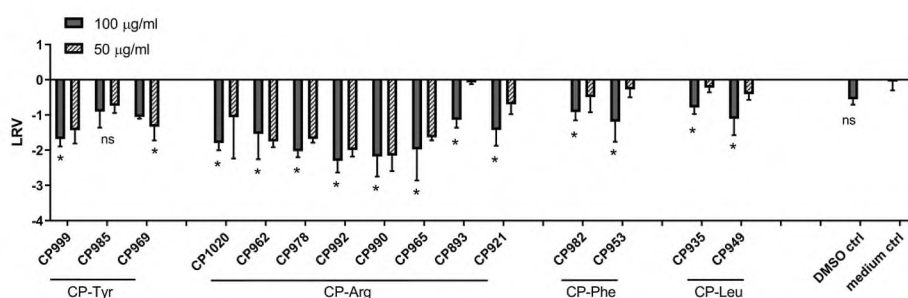
Fig. 4. Antiviral activity of cyanopeptolins isolated from *Nostoc edaphicum* CCNP1411 against Delta SARS-CoV-2. Virus replication was evaluated using quantitative RT-qPCR. Data are presented as Log Removal Value (LRV) compared to untreated samples (medium control). The assay was performed in triplicate, and average values with standard errors are presented (*$p < 0.05$).
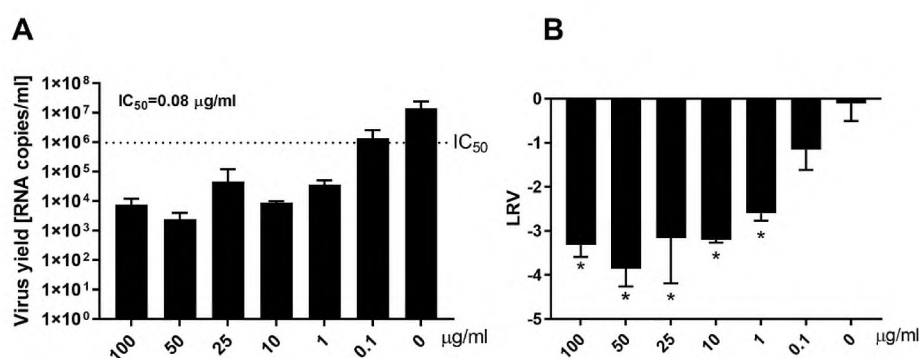
Fig. 5. Antiviral activity of cyanopeptolin CP978 isolated from *Nostoc edaphicum* CCNP1411 against SARS-CoV-2. Virus replication was evaluated using quantitative RT-q-PCR. Data are presented as viral yield (**A**) and Log Removal Value (LRV) compared to untreated samples (DMSO control) (**B**). The IC_{50} value was calculated using the GraphPad nonlinear regression (curve fit) analysis. The assay was performed in triplicate, and average values with standard errors are presented (*$p < 0.05$).

if CP978 hampers virus internalisation into cells. Likewise, no inhibitory effect of CP978 was observed. The "Adsorption assay", allowed to determine if the tested CP978 blocks the attachment of virus particles to the host cell. But also in this case no inhibition was observed, Then, the "Release assay", examined whether the cyanopeptolin hampers the late stages of SARS-CoV-2 replication, but no significant changes in the virus titer were observed. Simultaneously, an experiment with CP978 (50 µg/ml) or control (DMSO) present during all stages of virus infection was performed ("Normal assay"). As expected, in this experiment a strong decline in virus replication was observed (Fig. 6A). Lastly, the "Virus inactivation assay", verified the direct inactivation of the virus by the tested compound. The results showed a significant inhibition of SARS-CoV2 replication only in the case of the normal virus assay, with the cyanopeptolin present throughout the infection (Fig. 6A). However, here, a dramatic decrease in SARS-CoV-2 titer was observed after virus incubation with CP978, suggesting that the tested cyanopeptolin

interacts directly with the SARS-CoV-2 virions (Fig. 6B).

Next, we employed the primary HAE cultures (HAEs), which mimic the natural microenvironment of the respiratory tract. The results showed a great decline in SARS-CoV-2 replication in cells treated with CP978 (100 µg/ml) (Fig. 7A). These results were confirmed using primary cells from different donors, where SARS-CoV-2 infection was significantly diminished in the presence of 100 µg/ml of CP978 in all tested time points (Fig. 7B).

Next, the replication of different SARS-CoV-2 variants in the presence of CP978 was analysed. A standard infection assay was performed with Wuhan, Alpha, Omicron, and Delta (as control) variants ($TCID_{50} =$ 800/ml) in the presence of CP978 (50 µg/ml) or control (DMSO). The assay showed significant inhibition of all variants except Wuhan (Fig. 8A). Similarly, the inactivation assay showed inhibition of the Alpha, Omicron, and Delta variants, with no effect on Wuhan (Fig. 8B).

As SARS-CoV-2 was observed to be inhibited in direct interaction
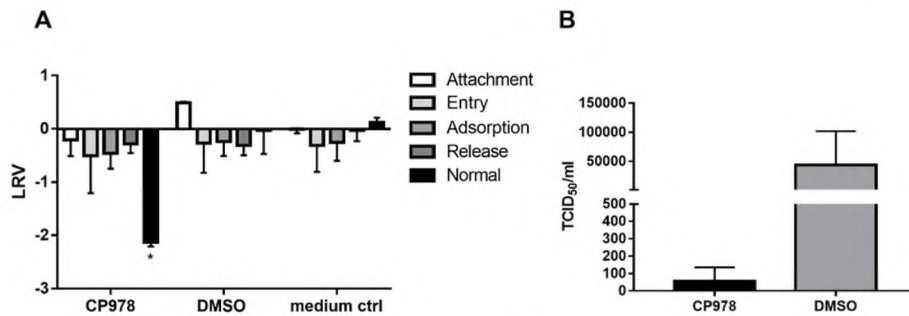
Fig. 6. The mechanism of action of cyanopeptolin CP978 isolated from *Nostoc edaphicum* CCNP1411. Mechanistic assays allowing recognition, at which stage the inhibition occurs. Virus replication was evaluated using quantitative RT-qPCR. Data are presented as Log Removal Value (LRV) compared to untreated samples (medium control). The assay was performed in triplicate, and average values with standard errors are presented (*$p < 0.05$) **(A)**. Inactivation assay showing a decrease in virus titer ($TCID_{50}$/ml) after incubation with CP978 or control (DMSO) **(B)**. The assay was performed in triplicate, and average values with standard errors are presented.
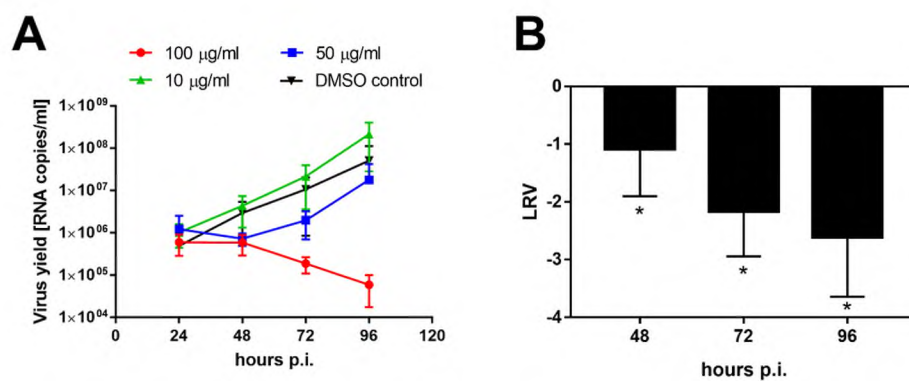
Fig. 7. Antiviral activity of cyanopeptolin CP978 isolated from *Nostoc edaphicum* CCNP1411 against Delta SARS-CoV-2 in HAEs. The kinetics of the virus replication was evaluated in the apical washes using quantitative RT-qPCR **(A)**. Data obtained using cells from three different donors are presented as Log Removal Value (LRV) compared to untreated samples (medium control) **(B)**. The assay was performed in triplicate, average values with standard errors are presented.
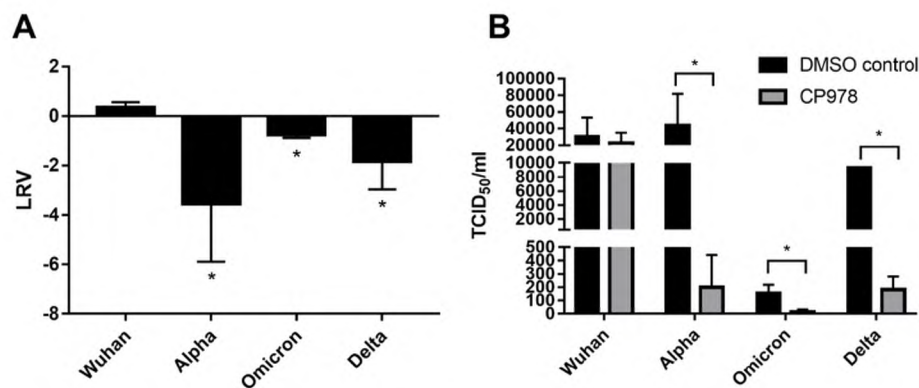
Fig. 8. Antiviral activity of cyanopeptolin CP978 against SARS-CoV-2 variants. Virus replication was evaluated using quantitative RT-qPCR. The data are presented as Log Removal Value (LRV) compared to untreated samples (medium control) **(A)** The assay was performed in triplicate, and average values with standard errors are presented (*$p < 0.05$). Inactivation assay showing a decline in virus titer ($TCID_{50}$/ml) after incubation with CP978 or control (DMSO) **(B)**. The assay was performed in triplicate, and average values with standard errors are presented (*$p < 0.05$).

with the CP978, we aimed to analyse how this affects virus binding to permissive cells. For this, virus adhesion was analysed with confocal microscopy. The results showed a great inhibition of SARS-CoV-2 binding to cells after incubation with CP978 (Fig. 9).

To verify whether the inhibition is S protein-dependent, we examined the entry of Delta SARS-CoV-2 pseudoviruses into the A549$^{ACE2/TMPRSS2}$ cells. VSV-G – decorated or naked (ΔEnv) pseudoviruses were used as a control. After 3 days of culture at 37 °C, pseudovirus entry was quantified by measuring the luciferase activity (Fig. 10). In the presence

of CP978, the entry of SARS-CoV-2-S pseudoviruses was significantly hampered, in contrast to VSV-G particles, which effectively infected under all cells conditions.

Lastly, the SARS-CoV-2 S protein interaction with the CP978 was confirmed with the application of MicroScale Thermophoresis (MST) assay. The determined affinity between the S protein and CP978 was estimated to be K_D of 3.8 μM (Fig. 11). This confirmed that the CP978-mediated inhibition of SARS-CoV-2 infection results from the direct binding of the cyanopeptolin with the coronaviral S protein.
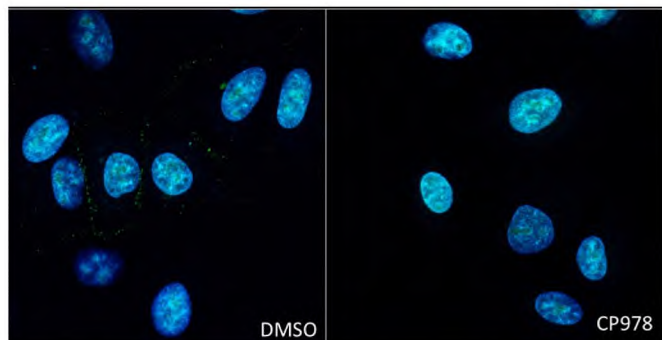
Fig. 9. Confocal analysis of SARS-CoV-2 adhesion in A549$^{ACE2/TMPRSS2}$ cells after pre-treatment with cyanopeptolin CP978 isolated from *Nostoc edaphicum* CCNP1411 or control (DMSO). The viral N protein was labelled with specific antibodies (green), and the nuclei were denoted in blue.
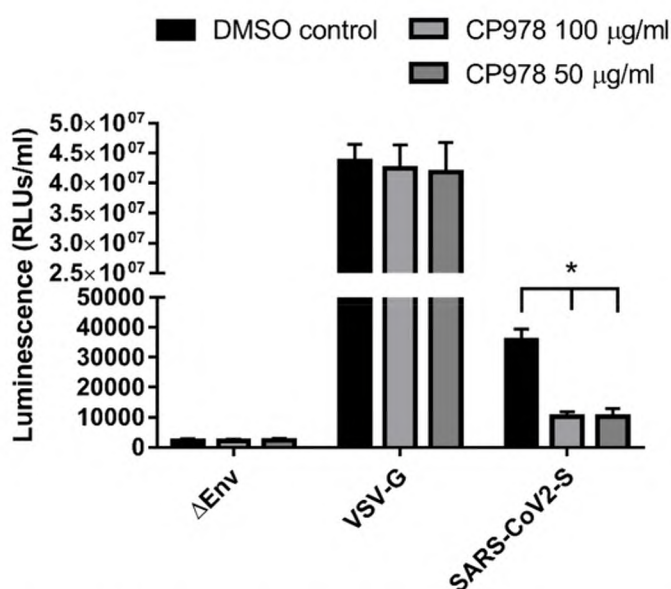
Fig. 10. Entry of the SARS-CoV-2 pseudoviruses in the presence of CP978 or control (DMSO). Data are presented as Relative Luminescence Units per ml. VSV-G – decorated or naked (ΔEnv) pseudoviruses were used as a controls. The assay was performed in triplicate, and average values with standard errors are presented (*$p < 0.05$).

4. Discussion

CPs are one of the most commonly occurring classes of cyanobacterial peptides. They have been identified in species from different cyanobacterial genera (e.g. *Microcystis*, *Planktothrix*, and *Nostoc*). In the CyanoMetDB database, 202 structural variants of these cyclic depsipeptides were deposited, including micropeptins, ichthyopeptins, aeruginopeptins and lyngbyastatins (Janssen et al., 2023; Jones et al., 2021). All these compounds contain a unique Ahp residue in position 3 and possess a side chain linked to Thr (optionally Pro) in position 1. In the side chain of many CPs, short fatty acids attached through glutamine (Gln), glutamic acid (Glu) or aspartic acids (Asp) are present. CP-like peptides were shown to inhibit the activity of serine proteases with selectivity and potency that depended mainly on the residue in position 2 linked to Ahp (Yamaki et al., 2022; Zainuddin et al., 2007; Mazur-Marzec et al., 2018). Despite their common occurrence in many bloom-forming cyanobacteria worldwide, not much has been reported on the activity of the peptides against other targets. Only in one study, the antiviral activity of ichthyopeptins, the CP-like peptides produced by
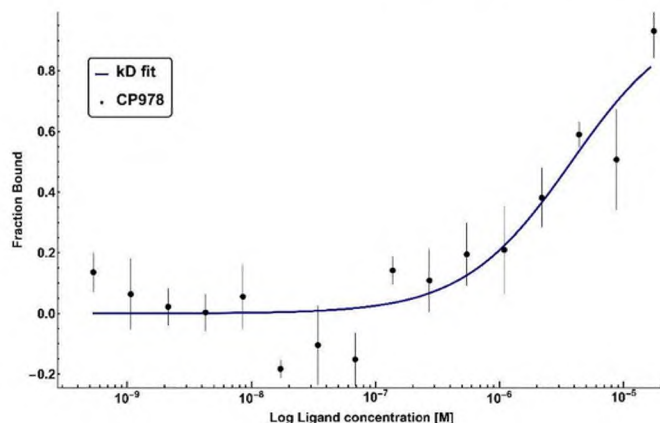
Fig. 11. The determination of affinity between the SARS-CoV-2 Spike ectodomain and cyanopeptolin CP978 isolated from *Nostoc edaphicum* CCNP1411 using MicroScale Thermophoresis. Experimental data (n = 3) is shown as black dots with measurement error as a bar. K_D fit is presented as a solid line.

Microcystis ichthyoblabe, was explored (Zainuddin et al., 2007). But even in that work, the fraction containing ichthyopeptins as the main components, not the isolated peptides, was tested. The samples (IC$_{50}$ = 12.5 μg/ml) protected the Madin-Darby canine kidney (MDCK) cells against influenza A (H1N1) virus-induced destruction, without cytotoxic effects on the cells. As the viral and cellular proteases are common targets of antiviral drugs, the authors suggested that the activity of the peptides can result from their inhibitory effects on the enzymes. Unfortunately, these studies have not been continued, so the antiviral potential of CP-like peptides has not been further explored.

In the current work, we isolated 15 cyanopeptolin variants. Two of the peptides lack a short fatty acid in a side chain, while in other CPs butanoic acid, hexanoic acid or acetyl group are present. The CPs also differ with respect to the residues in position 2 occupied by Arg, Tyr, Leu or Phe, and the residue in position 5 occupied by *N*- MeTyr, and *N,O*-diMeTyr or *N*-Phe. Thus far, these 15 CP variants were only identified in *N. edaphicum* CCNP1411 (Mazur-Marzec et al., 2018). A high number of structurally diverse CPs provided a good basis for further studies on the antiviral potential of this class of non-ribosomal peptides. It also allowed us to test the effect of the most variable residue in position 2 on the activity of the compounds. In the screening experiments, all CPs inhibited SARS-CoV-2 replication of in A549$^{ACE2/TMPRSS2}$ cells, but the most potent effects were recorded for Arg^2-containing peptides (LRV at 50 μg/ml from −1 to −2.5 logs). It was also revealed that Arg-containing CP variants lacking the fatty acid in the side chain either did not inhibit the SARS-CoV-2 infection at 50 μg/ml (CP983) or their LRV was low (−0.5 for CP922). This can indicate the contribution of both electrostatic and hydrophobic interactions between the molecule and its binding site. Optionally, the presence of the fatty acid chain can induce conformational changes in the peptide so that it fits better to the receptor. To gain knowledge about the significance of specific structural elements of CPs responsible for their antiviral activity, the CP target with its binding site and the structure of the whole complex should be determined.

For further studies on the antiviral potential of cyanopeptolins, the Arg-containing variant, CP978, produced by CCNP1411 in the highest amounts, was selected. In the virus infection assay, CP978 showed concentration-dependent inhibition of SARS-CoV-2 replication in A549$^{ACE2/TMPRSS2}$ cells. The determined IC$_{50}$ value was low (80 ng/ml = 82 nM), so that this variant can be classified into the natural products that most potently inhibit SARS-CoV-2 infection. In a review article by Wang et al. (2022), the IC$_{50}$ values for anti-SARS-CoV-2 natural products ranges from 0.028 μM for the cathepsin L inhibitor, gallinamide A isolated from marine cyanobacterium *Schizothrix* (Ashhurst et al., 2022), to 8.1 μM for the wallichin D, the 3Clpro inhibitor from *Dryopteris wallichiana* (Hou et al., 2021). The IC$_{50}$ value of CP978 is also low, compared

to many other tested SARS-CoV-2 inhibitors (Xiang et al., 2022; Chen et al., 2022; Hurst et al., 2021; Milewska et al., 2021; Jo et al., 2020).

The potential of CP978 as an anti-SARS-CoV-2 agent was additionally documented in a 3D cell culture model with HAE cells. In our tests, CP978 significantly inhibited the replication of SARS-CoV-2 in the ACE2-expressing HAE cells. HAE constitutes a frontline defence system against inhaled pathogens, including viruses. In culture, HAEs form a pseudostratified epithelial layer with many functional cell types, effectively mimic the natural respiratory track microenvironment. Therefore, they are used as physiologically relevant models for the anti-SARS-CoV-2 drug screening and studies of viral pathology (Mulay et al., 2021).

A series of functional assays performed in this study indicated a direct interaction of CP978 with viral particles. This mode of action was also confirmed with application of confocal microscopy. After virus pre-exposure to CP978, no SARS-CoV-2 adhesion in A549$^{ACE2/TMPRSS2}$ cells was observed. Generally, compounds that act extracellularly, and affect the early stages of viral infection, are especially valuable as antiviral drug candidates (Schütz et al., 2020; Lee et al., 2022; Moroy and Tuffery, 2022). This mode of action reduces the potential risk of negative side effects induced by antivirals, after they enter into the cell. Compounds that interact with ACE2 can be effective against different SARS-CoV-2 mutants and usually show a wider spectrum of antiviral activity. However, this mode of action can disrupt the natural function of the receptor and induce adverse effects in cells (Jia et al., 2020).

The studies revealed differences in the response of the four variants of SARS-CoV-2, Wuhan, Alpha, Omicron and Delta, to cyanopeptolin CP978. Most significant mutations in the virus were usually recorded in the spike protein and led to the appearance of new variants of concern (VOC) (Abavisani et al., 2022; Koley et al., 2022). The S protein is a homotrimer composed of three monomeric structures with an *N*-terminal signal peptide and two functional subunits, S1 and S2. These subunits participate in the binding of viral particles to the host cellular receptor (S1) and in the fusion of viral and host cellular membranes (S2). The S1 is a highly glycosylated subunit with a receptor-binding domain (RBD) which interacts directly with ACE2 (Walls et al., 2020). Mutations in RBD are critical for the binding affinity to ACE2 of the host cell and for the infectivity of the virus (da Costa et al., 2022). In our study, the role of the S protein in the interaction of CP978 with SARS-CoV-2 was proven in the cell entry assays. In the assay, the recombinant human immunodeficiency virus pseudotyped with the SARS-CoV-2 S protein, vesicular stomatitis virus G protein or with the particles padoneicles particles lacking the fusion protein were used. The inhibition of SARS-CoV-2-S pseudovirus entry into A549$^{ACE2/TMPRSS2}$ cells by CP978 and the effective infection of the cells by VSV-G particles strongly indicated the interaction of CP978 with the viral S protein. This mode of the cyanopeptolin action was additionally confirmed by the microscale thermophoresis assay with S protein. The determined dissociation constant suggests a strong binding interaction of CP978 with the SARS-CoV-2 S protein. The differences in CP978 activity against Wuhan and other variants are most likely related to the amino acid mutations in the S protein.

Natural compounds, including peptides, are extensively explored in the search for new therapeutics for the treatment and prevention of viral infections. Peptides, especially those positively charged and amphipathic, are considered good antiviral drug candidates (Schütz et al., 2020; Lee et al., 2022; Moroy and Tuffery, 2022). They are characterised by high efficacy, safety and specificity. In the case of the non-ribosomal peptides, composed of non-proteinogenic residues, such as cyanopeptolins, they are additionally less prone to proteolytic cleavage and have improved stability. These compounds also show potent activity against many serine proteases, and therefore they can find application as multi-target therapeutics.

5. Conclusions

COVID-19 pandemics had devastating effects on different areas of our lives. Considering the fact that current methods for effective treating the infection are limited and the risk of new outbreaks of the diseases exists, the attempts to develop new anti-SARS-CoV-2 agents should continue. Cyanopeptolins isolated from *Nostoc edaphicum* CCNP1411 are among the compounds that could be considered for further studies. The tested CP978 was found to be effective against three, more recently evolved variants of SARS-CoV-2 and showed a low inhibitory concentration value. So far, no cytotoxic effects of the peptides have been recorded. Additionally, the mode of CP978 action, through binding to the S protein, decreases the risk of potential side effects in the treated cells. The discovery of the exact location of CP978 binding site to the S protein would facilitate the process of peptide modification into compounds with a broader spectrum of antiviral activity and possibly simpler structure.

Author contributions

RK, HMM, AM and KP conceived and designed the overall study. RK cultured cyanobacteria, carried out the extraction, isolation and purification of cyanopeptolins, performed the LC-MS/MS analyses. RK and HMM elucidated the CPs structures. EW performed the NMR analysis. SI, TK and RK performed HRMS analysis. AM conceived all biological research and performed the antiviral assays under the supervision of KP. NDTD performed RT-qPCR analyses. JP performed MST analyses. EBD participated in cell culture preparation. AS performed confocal microscopy analysis. DJ and JN provided materials for the study. KP supervised the study. RK wrote the manuscript with the input from all co-authors. All authors reviewed the manuscript.

Declaration of competing interest

The authors declare that they have no known competing financial interests or personal relationships that could have appeared to influence the work reported in this paper.

Data availability

Data will be made available on request.

Appendix A. Supplementary data

Supplementary data to this article can be found online at https://doi. org/10.1016/j.antiviral.2023.105731.

References

Abavisani, M., Rahimian, K., Mahdavi, B., Tokhanbigli, S., Siasakht, M.M., Farhadi, A., Kodori, M., Mahmanzar, M., Meshkat, Z., 2022. Mutations in SARS-CoV-2 structural proteins: a global analysis. Virol. J. 19, 220. https://doi.org/10.1186/s12985-022-01951-7.

Al-Harrasi, A., Behl, T., Upadhyay, T., Chigurupati, S., Bhatt, S., Sehgal, A., Bhatia, S., Singh, S., Sharma, N., Vijayabalan, S., Palanimuthu, V.R., Das, S., Kaur, R., Aleya, L., Bungau, S., 2022. Targeting natural product against SARS-CoV-2. ESPR 29, 42404–42432. https://doi.org/10.1007/s11356-022-19770-2.

Ashhurst, A.S., Tang, A.H., Fajtová, P., Yoon, M.C., Aggarwal, A., Bedding, M.J., Stoye, A., Beretta, L., Pwee, D., Drelich, A., Skinner, D., Li, L., Meek, T.D., McKerrow, J.H., Hook, V., Tseng, C.-T., Larance, M., Turville, S., Gerwick, W.H., O'Donoghue, A.J., Payne, R.J., 2022. Potent Anti-SARS-CoV-2 Activity by the natural product gallinamide A and analogues via inhibition of cathepsin L. J. Med. Chem. 65 (4), 2956–2970. https://doi.org/10.1021/acs.jmedchem.1c01494.

Barreto-Duran, E., Szczepański, A., Gałuszka-Bulaga, A., Surmiak, M., Siedlar, M., Sanak, M., Rajfur, Z., Milewska, A., Lenart, M., Pyrć, K., 2022. The interplay between

the airway epithelium and tissue macrophages during the SARS-CoV-2 infection. Front. Immunol. 13, 991991. https://doi:10.3389/fimmu.2022.991991.

Barrientos, L.G., O'Keefem, B.R., Bray, M., Sanchez, A., Gronenborn, A.M., Boyd, M.R., 2003. Cyanovirin-N binds o the viral surface glycoprotein $GP_{1,2}$ and inhibits infectivity of Ebola virus. Antivir. Res. 58, 47–56. https://doi.org/10.1016/S0166-3542(02)00183-3.

Barrientos, L.G., Gronenborn, A.M., 2005. The highly specific carbohydrate-binding protein cyanovirin-N: structure, anti-HIV/ebola activity and possibilities for therapy. Mini-Rev. Med. Chem. 5, 21–31. https://doi.org/10.2174/1389557053402783.

Beigel, J.H., Tomashek, K.M., Dodd, L.E., Mehta, A.K., Zingman, B.S., Kalil, A.C., Hohmann, E., Chu, H.Y., Luetkemeyer, A., Kline, S., Lopez de Castilla, D., Finberg, R. W., Dierberg, K., Tapson, V., Hsieh, L., Patterson, T.F., Paredes, R., Sweeney, D.A., Short, D.A., Touloumi, G., Lye, D.C., Ohmagari, N., Oh, M., Ruiz-Palacios, G.M., Benfield, T., Fätkenheuer, G., Kortepeter, M.G., Atmar, R.L., Creech, C.B., Lundgren, J., Babiker, A.G., Pett, S., Neaton, J.D., Burgess, T.H., Bonnett, T., Green, M., Makowski, M., Osinusi, A., Nayak, S., Lane, H.C., 2020. Remdesivir for the treatment of covid-19 – final report. N. Engl. J. Med. 383, 1813–1826. https://doi.org/10.1056/NEJMoa2007764.

Cao, L., Lou, J., Chan, S.Y., Zheng, H., Liu, C., Zhao, S., Li, Q., Mok, C.K.P., Chan, R.W.Y., Chong, M.K.C., Wu, W.K.K., Chen, Z., Wong, E.L.Y., Chan, P.K.S., Zee, B.C.Y., Yeoh, E.K., Wang, M.H., 2022. Rapid evaluation of COVID-19 vaccine effectiveness against symptomatic infection with SARS-CoV-2 variants by analysis of genetic distance. Nat. Med. 28, 1712–1722. https://doi.org/10.1038/s41591-022-01877-1.

Carpine, R., Sieber, S., 2021. Antibacterial and antiviral metabolites from cyanobacteria: their application and their impact on human health. CRBIOT 3, 65–81. https://doi.org/10.1016/j.crbiot.2021.03.001.

Chen, Y., Wu, S., Chen, S., Zhan, Q., Wu, D., Yang, C., He, X., Qiu, M., Zhang, N., Li, Z., Guo, Y., Wen, M., Lu, L., Ma, C., Guo, J., Xu, W., Li, X., Li, L., Jiang, S., Pan, X., Liu, S., Suiyi, T., 2022. Sertraline Is an Effective SARS-CoV-2 Entry Inhibitor Targeting the Spike Protein, vol. 96, e0124522. https://doi.org/10.1128/jvi.01245-22.

Chhetri, B.K., Tedbury, P.R., Sweeney-Jones, A.M., Mani, L., Soapi, K., Manfredi, C., Sorscher, E., Sarafianos, S.G., Kubanek, J., 2022. Marine natural products as leads against SARS-CoV-2 infection. J. Nat. Prod. 85, 657–665. https://doi.org/10.1021/acs.jnatprod.2c00015.

COVID-19 Excess Mortality Collaborators, 2022. Estimating excess mortality due to the COVID-19 pandemic: a systematic analysis of COVID-19-related mortality, 2020–2021. Lancet 339, 1513–1536. https://doi.org/10.1016/S0140-6736(21)02796-3.

da Costa, C.H.S., de Freitas, C.A.B., Alves, C.N., Lameira, J., 2022. Assessment of mutations on RBD in the spike protein of SARS-CoV-2 Alpha, Delta and Omicron variants. Sci. Rep. 12, 8540. https://doi.org/10.1038/s41598-022-12479-9.

da Silva Antonio, A., Moreira Wiedemann, L.S., Veiga-Junior, V.F., 2020. Natural products' role against COVID-19. RSC Adv. 10, 23379–23393. https://doi.org/10.1039/d0ra03774e.

Gademann, K., Portmann, C., Blom, J.F., Zeder, M., Jüttner, F., 2010. Multiple toxin production in the cyanobacterium *Microcystis*: isolation of the toxic protease inhibitor cyanopeptolin 1020. J. Nat. Prod. 73, 980–984. https://doi.org/10.1021/np900818c.

Gesner-Apter, S., Carmeli, S., 2009. Protease inhibitors from a water bloom of the cyanobacterium *Microcystis aeruginosa*. J. Nat. Prod. 72, 1429–1436. https://doi.org/10.1021/np900340t.

Hou, B., Zhang, Y.-M., Liao, H.-Y., Fu, L.-F., Zhao, X., Qi, J.-X., Yang, W., Xiao, G.-F., Yang, L., Zuo, Z.-Y., Wang, L., Zhang, X.-L., Bai, F., Yang, L., Gao, G.F., Song, H., Hu, J.-M., Shang, W.-J., Zhou, J., 2021. Target-based virtual screening and LC/MS-guided isolation procedure for identifing phloroglucinol-terpenoid inhibitors of SARS-CoV-2. J. Nat. Prod. 85 (2), 327–336. https://doi.org/10.1021/acs.jnatprod.1c00805.

Hurst, B.L., Dickinson, D., Hsu, S., 2021. Epigallocatechin-3-gallate (EGCG) inhibits SARS-CoV-2 infection in primate epithelial cells. Microbiol. Infect. Dis 5, 2. https://doi.org/10.33425/2639-9458.1116.

Janssen, E.M.-L., Jones, M.R., Pinto, E., Dörr, F., Torres, M.A., Rios, J.F., Mazur-Marzec, H., Szubert, K., Konkel, R., Tartaglione, L., Dell'Aversano, C., Miglione, A., McCarron, P., Beach, D.G., Miles, C.O., Fewer, D.P., Sivonen, K., Jokela, J., Wahlsten, M., Niedermeyer, T.H.J., Schanbacher, F., Leão, P., Preto, M., D'Agostino, Paul M., Baunach, M., Dittmann, E., Reher, R., 2023. CyanoMetDB Version02: Comprehensive Database of Secondary Metabolites from Cyanobacteria. https://doi.org/10.1016/j.watres.2021.117017.

Jia, H., Neptune, E., Cui, H., 2020. Targeting ACE2 for COVID-19 therapy: opportunities and challenges. Am. J. Respir. Cell Mol. Biol. 64 (4), 416–425. https://doi.org/10.1165/rcmb.2020-0322PS.

Jo, S., Kim, S., Kim, D.Y., Kim, M.-S., Shin, D.H., 2020. Flavonoids with inhibitory activity against SARS-CoV-2 3CLpro. J. Enzym. Inhib. Med. Chem. 35 (1), 1539–1544. https://doi.org/10.1080/14756366.2020.1801672.

Jones, M., Pinto, E., Torres, M.A., Dörr, F., Mazur-Marzec, H., Szubert, K., Tartaglione, L., Dell'Aversano, C., Miler, C.O., Beach, D.G., McCarron, P., Sivonen, K., Fewer, D.P., Jokela, J., Janssen, E.M.-L., 2021. CyanoMetDB, a comprehensive public database of secondary metabolites from cyanobacteria. Water Res. 196, 117017. https://doi.org/10.1016/j.watres.2021.117017.

Kanekiyo, K., Hayashi, K., Takenaka, H., Lee, J.-B., Hayashi, T., 2007. Anti-herpes simplex virus target of an acidic polysaccharide, nostoflan, from the edible blue-green alga *Nostoc flagelliforme*. Biol. Pharm. Bull. (Arch. Am. Art) 30, 1573–1575. https://doi.org/10.1248/bpb.30.1573.

Koley, T., Goswami, A., Kumar, M., Upadhyyay, N., Hariprasad, G., 2022. Comparative structural analysis of human ACE2 receptor with spike protein of SARS-CoV-2

variants: implications to understand infectivity of the virus. Adv. Appl. Bioinforma. Chem. 15, 21–27. https://doi.org/10.2147/AABC.S360787.

Kotai, J., 1972. Instructions for Preparation of Modified Nutrient Solution Z8 for Algae; Publication: B-11/69; Norwegian Institute for Water Research: Oslo, Norway, p. 5.

Krumm, Z., Lloyd, G.M., Francis, C.R., Nasif, L.H., Mitchell, D.A., Golde, T.E., Giasson, B. I., Xia, Y., 2021. Precision therapeutic targets for COVID-19. Virol. J. 18, 66. https://doi.org/10.1186/s12985-021-01526-y.

Lee, W., Rahimi, M., Lee, Y., Chiu, A., 2021. POKY: a software suite for multidimensional NMR and 3D structure calculation of biomolecules. Bioinformatics 37, 3041–3042. https://doi.org/10.1093/bioinformatics/btab180.

Lee, Y.-C., Shirkey, J.D., Park, J., Bisht, K., Cowan, A.J., 2022. An overview of antiviral peptides and rational biodesign consideration. BioDesign Research. https://doi.org/10.34133/2022/9898241, 9898241.

Liu, J., Pan, X., Zhang, S., Li, M., Ma, K., Fan, C., Lv, Y., Guan, X., Yang, Y., Ye, X., Deng, X., Wang, Y., Qin, L., Xia, Z., Zhou, Q., Zhang, X., Ling, Y., Qi, T., Wen, Z., Huang, S., Zhang, L., Wang, T., Liu, Y., Huang, Y., Li, W., Du, H., Chen, Y., Xu, Y., Zhao, Q., Zhao, R., Annane, D., Qu, J., Chen, D., 2023. Eficacy and safety of Paxlovid in severe adult patients with SARS-Cov-2 infection: a multicentre randomizezd controlled study. The Lancet Regional Health – Western Pacific 33, 100694. https://doi.org/10.1016/j.lanwpc.2023.100694.

Liu, Y., Caroll, J.R., Holt, L.A., McMahon, J., Giomarelli, B., Ghirlanda, G., 2009. Multivalent interactions with gp120 are required for the anti-HIV activity of cyanovirin. Biopolymers 92 (3), 194–200. https://doi.org/10.1002/bip.21173.

Lv, Z., Cano, K.E., Jia, L., Drag, M., Huang, T.T., Olsenm, S.K., 2022. Targeting SARS-CoV-2 proteases for COVID-10 antiviral development. Front. Chem. 9, 819165. https://doi.org/10.3389/fchem.2021.819165.

Mader, J., Gallo, A., Schommartz, T., Handke, W., Nagel, C.-H., Günther, P., Brune, W., Reich, K., 2016. Calcium spirulan derived from *Spirulina platensis* inhibits herpes simplex virus 1 attachment to human keratinocytes and protects against herpes labialis. J. Allergy Clin. Immunol. 137, 197–203. https://doi.org/10.1016/j.jaci.2015.07.027.

Mazur-Marzec, H., Cegłowska, M., Konkel, R., Pyrć, K., 2021. Antiviral cyanomebolites-A review. Biomolecules 11, 474. https://doi.org/10.3390/biom11030474.

Mazur-Marzec, H., Fidor, A., Cegłowska, M., Wieczerzak, E., Kropidłowska, M., Goua, M., Macaskill, J., Edwards, C., 2018. Cyanopeptolins with trypsin and chymotrypsin inhibitory activity from the cyanobacterium *Nostoc edaphicum* CCNP1411. Mar. Drugs 16, 220. https://doi.org/10.3390/md16070220.

Milewska, A., Chi, Y., Szczepanski, A., Barreto-Duran, E., Dabrowska, A., Botwina, P., Obloza, M., Liu, K., Liu, D., Guo, X., Ge, Y., Li, J., Cui, L., Ochman, M., Urlik, M., Rodziewicz-Motowidło, S., Zhu, F., Szczubialka, K., Nowakowska, M., Pyrć, K., 2021. HTCC as a polymeric inhibitor of SARS-CoV-2 and MERS-CoV. J. Virol. 95, e01622-20. https://doi.org/10.1128/JVI.01622-20.

Milewska, A., Falkowski, K., Kulczycka, M., Bielecka, E., Naskalska, A., Mak, P., Lesner, A., Ochman, M., Urlik, M., Diamandis, E., Prassas, I., Potempa, J., Kantyka, T., Pyrć, K., 2020. Kallikrein 13 serves as a priming protease during infection by the human coronavirus HKU1. Sci. Signal. 13, eaba9902. https://doi:10.1126/scisignal.aba9902.

Mitchell, C.A., Ramessar, K., O'Keefe, B.R., 2017. Antiviral lectins: selective inhibitors of viral entry. Antivir. Res. 142, 37–54. https://doi.org/10.1016/j.antiviral.2017.03.007.

Moroy, G., Tuffery, P., 2022. Peptide-based strategies against SARS-CoV-2 attack: an undated *in Sillico* perspective. Front. Drug. Discov 2, 899477. https://doi.org/10.3389/fddsv.2022.899477.

Mulay, A., Konda, B., Garcia Jr., G., Yao, C., Beil, S., Vilalba, J.M., Koziol, C., Sen, C., Purkayastha, A., Kolls, J.K., Pociask, D.A., Pessina, P., de Aja, J.S., Garcia-de-Alba, C., Kim, C.F., Gomperts, B., Arumugaswami, V., Stripp, B.R., 2021. SARS-CoV-2 infection of primary human lung epithelium for COVID-19 modeling and discovery. Cell Rep. 25, 109055. https://doi.org/10.1016/j.celrep.2021.109055.

Naidoo, D., Roy, A., Kar, P., Mutanda, T., Anadraj, A., 2020. Cyanobacterial metabolites as promising drug leads against the M^{pro} and PL^{pro} of SARS-CoV-2: an *in sillico* analysis. J. Biomol. Struct. Dyn. 39, 6218–6230. https://doi.org/10.1080/07391102.2020.1794972.

Petit, L., Vernès, L., Cadoret, J.-P., 2021. Docking and in silico toxicity assessment of *Arthrospira* compounds as potential antiviral agents against SARS-CoV-2. J. Appl. Phycol. 33, 1579–1602. https://doi.org/10.1007/s10811-021-02372-9.

Raman, K., Rajagopal, K., Islam, F., Dhawan, M., Mitra, S., Aparna, B., Varakumar, P., Byran, G., Groudhary, O.P., Emran, T.B., 2022. Role of natural products towards the SARS-CoV-2: a critical review. Ann. Med. Surg 80, 104062. https://doi.org/10.1016/j.amsu.2022.104062.

Reed, J.J., Muench, H., 1938. A simple method of estimating fifty per cent endpoints. Am. J. Hyg. 27, 3. https://doi.org/10.1093/oxfordjournals.aje.a118408.

Rommasi, F., Nasiri, M.J., Mirsaeidi, M., 2022. Immunomodulatory agents for COVID-19 treatment: possible mechanism of action and immunopathology features. Mol. Cell. Biochem. 477, 711–726. https://doi.org/10.1007/s11010-021-04325-9.

Saad, M.H., El-Fakharany, E.M., Salem, M.S., Sidkey, N.M., 2020. *In vitro* assessment of dual (antiviral and antitumor) activity of a novel lectin produced by the newly cyanobacterium isolate, *Oscillatoria acuminate* MHM-632 MK01410.1 J. Biomol. Struct. Dyn 40 (8), 3560–3580. https://doi.org/10.1080/07391102.2020.1848632.

Sahu, N., Mishra, S., Kesheri, M., Kanchan, S., Sinha, R.P., 2022. Identification of cyanobacteria-based natural inhibitors against SARS-CoV-2 druggable target ACE2 using molecular docking study, ADME and toxicity analysis. Indian J. Clin. Biochem. 38, 361–373. https://doi.org/10.1007/s12291-022-01056-6.

Schütz, D., Ruiz-Blanco, Y.B., Münch, J., Kirchhoff, F., Sanchez-Garcia, E., Müller, J.A., 2020. Peptide and peptide-based inhibitors of SARS-CoV-2 entry. Adv. Drug Deliv. Rev. 167, 47–65. https://doi.org/10.1016/j.addr.2020.11.007.

Shapira, T., Monreal, A.I., Dion, S.P., Buchholz, D.W., Imbiakha, B., Olmstead, A.D., Jager, M., Désilets, A., Gao, G., Martins, M., Vandal, T., Thompson, C.A.H., Chin, A., Rees, W.D., Steiner, T., Nabi, I.R., Marsault, E., Sahler, J., Diel, D.G., Van de Walle, G.R., August, A., Whittaker, G.R., Boundreault, P.-L., Leduc, R., Aguilar, H.C., Jean, F., 2022. A TMPRSS2 inhibitor acts a pan-SARS-CoV-2 prophylactic and therapeutic. Nature 605, 340. https://doi.org/10.1038/s41586-022-04661-w.

Synowiec, A., Jedrysik, M., Branicki, W., Klajmon, A., Lei, J., Owczarek, K., Suo, C., Szczepanski, A., Wang, J., Zhang, P., Labaj, P.P., Pyrc, K., 2021. Identyfication of cellular factors required for SARS-CoV-2 replication. Cells 10, 3159. https://doi.org/10.3390/cells10113159.

Vargas, P.-V., Shapira, T., Olmstead, A.D., Villanueva, I., Thompson, C.A.H., Ennis, S., Gao, G., de Guzman, J., Williams, D.E., Wang, M., Chin, A., Baustista-Sánchez, D., Agafitei, O., Levett, P., Xie, X., Nuzzo, G., Freire, V.F., Quintana-Bulla, J.I., Bernardi, D.I., Gubiani, J.R., Suthiphasilp, V., Raksat, A., Meesakul, P., Polbuppha, I., Chaiyosang, B., Teles, H.L., Manzo, E., Fontana, A., Leduc, R., Boudreault, P.-L., Berlinck, R.G.S., Laphookkhieo, S., Kanokmedhakul, S., Tietjen, I., Cherhasov, A., Krajden, M., Nabi, I.R., Niikura, M., Shi, P.-Y., Andersen, R.J., Jean, F., 2023. Discovery of lead natural products for developing pan-SARS-CoV-2 therapeutics. Antivir. Res. 209, 105484. https://doi.org/10.1016/j.antiviral.2022.105484.

Walls, A.C., Park, Y.-J., Tortorici, M.A., Wall, A., McGuire, A.T., Veesler, D., 2020. Structure, function, and antigenicity of the SARS-CoV-2 spike glycoprotein. Cell 180, 281–292. https://doi.org/10.1016/j.cell.2020.02.058.

Wang, Z., Wang, N., Yang, L., Song, Z-q, 2022. Bioactive natural products in COVID-19 therapy. Front. Pharmacol. 13, 926507. https://doi.org/10.3389/fphar.2022.926507.

Xiang, R., Yu, Z., Wang, Y., Wang, L., Huo, S., Li, Y., Liang, R., Hao, Q., Ying, T., Gao, Y., Yu, F., Jiang, S., 2022. Recent advances in developing small-molecule inhibitors against SARS-CoV-2. Acta Pharm. Sin. B. 12 (4), 1591–1623. https://doi.org/10.1016/j.apsb.2021.06.016.

Yamaki, H., Sitachitta, N., Sano, T., Kaya, K., 2022. Two new chymotrypsin inhibitors isolated from the cyanobacterium *Microcystis aeruginosa* NIES-88. J. Nat. Prod. 68, 14–18. https://doi.org/10.1021/np0401361.

Yip, A.J.W., Low, Z.Y., Chow, V.T.K., Lal, S.L., 2022. Repurposing molnupiravir for COVID-19: the mechanisms of antiviral activity. Viruses 14, 1345. https://doi.org/10.3390/v14061345.

Zainuddin, E., Mentel, R., Wray, V., Jansen, R., Nimtz, M., Lalk, M., Mundi, S., 2007. Cyclic depsipeptides, ochthyopeptins A and B, from *Microcystis ichthyoblabe*. J. Nat. Prod. 70, 1084–1088. https://doi.org/10.1021/np060303s.

Zeng, B., Gao, L., Zhou, Q., Yu, K., Sun, F., 2022. Effectiveness of COVID-19 vaccines against SARS-CoV-2 variants of concern: a systematic review and meta-analysis. BMC Med. 20, 200. https://doi.org/10.1186/s12916-022-02397-y.